Quantification of structural response and edge orientation of Chopped Tape Thermoplastic Composites in net-shaped specimens

Gulmez, Deniz Ezgi; Maldonado, Jesus; Masania, Kunal; Sinke, Jos; Dransfeld, Clemens

DOI
10.1016/j.compstruct.2023.117302

Publication date
2023

Document Version
Final published version

Published in
Composite Structures

Citation (APA)
Gulmez, D. E., Maldonado, J., Masania, K., Sinke, J., & Dransfeld, C. (2023). Quantification of structural response and edge orientation of Chopped Tape Thermoplastic Composites in net-shaped specimens. *Composite Structures*, *321*, Article 117302. https://doi.org/10.1016/j.compstruct.2023.117302

Composite Structures 321 (2023) 117302

Contents lists available at ScienceDirect

Composite Structures

journal homepage: www.elsevier.com/locate/compstruct

Quantification of structural response and edge orientation of Chopped Tape Thermoplastic Composites in net-shaped specimens

Deniz Ezgi Gulmez [a,*], Jesus Maldonado [b], Kunal Masania [a], Jos Sinke [a], Clemens Dransfeld [a,*]

[a] Department of Aerospace Structures & Materials, Faculty of Aerospace Engineering, Delft University of Technology, Kluyverweg 1, Delft 2629 HS, The Netherlands
[b] Institute of Polymer Engineering, FHNW University of Applied Sciences and Arts Northwestern Switzerland, CH-5210, Windisch, Switzerland

ARTICLE INFO

Keywords:
Chopped Tape Composites
Net-shaped specimens
Orientation tensor
Stiffness model

ABSTRACT

Chopped Tape Thermoplastic Composites (CTTCs) offer high formability and performance for complex-shaped components in the aerospace and automotive industries. However, the mesoscopic discontinuity leads to spatial variabilities and correspondingly high scatter in the elastic properties of CTTCs due to the random orientations of chopped tapes and chopped tape-cavity edge interactions. Here we propose a new approach to investigate the effect of mould cavity edges on chopped tape orientation and hence the mechanical properties of CTTCs. Based on this approach, a Set Voronoi tessellation was implemented to represent the variability of local Young's Modulus and chopped tape-cavity edge interactions occurring during the manufacturing process. It was confirmed that the chopped tapes align along the edges, and progressively transition to a random orientation towards the middle of the specimen. The results were validated on moulded specimens and demonstrated the ability to deconvolute the edge interaction.

1. Introduction

The need for reducing carbon emissions in the aerospace and automotive industries is leading to the broader adoption of lightweight structures in primary structures and secondary structures [1,2]. Most aerospace and automotive structures are made of continuous fibre composites whereas complex-shaped structures are generally produced by metalworking due to their elaborate shapes and complex load paths [3,4]. The need to manufacture lightweight structures and to reduce energy consumption and production cost has increased the interest in using fibre-reinforced composite materials. However, the limited formability of continuous fibre composites and the low performance of short fibre composites motivate research on novel composite material architectures for complex and net-shaped parts. For example, Chang and Pratte [5] showed the relative relation between processability and mechanical performance of fibre-reinforced composites according to their fibre architectures.

Referred to as Discontinuous Long Fibres (DLF) [5], Randomly Oriented Strands (ROS) [6,7], Tow-Based Discontinuous Composites (TBDCs) [8], pre-preg platelets [9,10], chopped carbon fibre tape-reinforced thermoplastics (CTT) [11–13], flake-based and ribbon-based composites or, as in this study chopped tapes thermoplastic composites (CTTCs) composites, there has been great interest in the structure–property relations of CTTCs. Their architectures offer a significant processability advantage compared to continuous fibre reinforcement without compromising their desirable high fibre volume fraction [5]. However, the prediction of the mechanical response of CTTCs poses challenges due to the anisotropy and spatial variability of the structures. Researchers have developed numerous modelling approaches to generate structural models and estimate their mechanical response [7,10,14–21]. Despite these many existing modelling techniques, the effects of the mould edges on the orientation of the chopped tapes have been found to limited attention. Tuttle et al. [22] showed experimentally that specimens at the edges have high stiffness compared to the specimens from the centre region of a moulded plate. On the other hand, component-level manufacturing has been getting attention to minimise or eliminate production waste due to environmental impacts, and circularity [23–26]. Understanding the effect of the cavity on material orientations is essential in optimising component-level manufacturing for minimum production waste and environmental impact. By gaining a better understanding of this cavity effect, manufacturers can more effectively control the manufacturing process and material performance while reducing material waste.

Capturing these materials' stochastic structure is relevant to understanding their response. The Random Sequential Adsorption (RSA) algorithm is a popular method to generate the distribution of CTTCs. Particles are positioned without overlapping each other until a desired number of particles is jammed or a defined number of attempts is

* Corresponding authors.
E-mail addresses: D.E.Gulmez@tudelft.nl (D.E. Gulmez), C.A.Dransfeld@tudelft.nl (C. Dransfeld).

https://doi.org/10.1016/j.compstruct.2023.117302
Received 28 February 2023; Received in revised form 14 May 2023; Accepted 21 June 2023
Available online 30 June 2023

attained [27]. There is no geometrical limitation for particles in the RSA algorithm to generate a dispersion of spherical particles [27], rods or single fibres [28–31] and rectangular particles or chopped tapes [32]. In their study about the distribution of cylindrical particles, Evans and Ferrar [33] examined the effect of the ratio between fibre diameter and length (aspect ratio) on orientation freedom and fibre volume ratio and showed that the high aspect ratio reduces the packing fraction due to a high angular misalignment which causes considerable gaps between fibres. When it comes to the application of the RSA algorithm for CTTCs, Chen et al. [32] modified the RSA algorithm to achieve a high fibre volume fraction by increasing the overlap freedom. However, in the above work, the boundaries of the distribution area were not defined in the RSA algorithm, making it problematic to obtain a realistic distribution considering the chopped tape dimension in relation to a mould cavity dimension.

The general RSA algorithm is not sufficient to limit the boundary of the mould cavity and to define the full distribution of the tapes. Li et al. [34] developed a reconstruction approach to establish the 'process-structure–property' relationships by applying a Voronoi tessellation algorithm that divides the Representative Volume Element (RVE) into subregions that have variable area and orientation information. Feraboli et al. [35] improved a stochastic laminate method to evaluate the average axial modulus of equivalent quasi-isotropic laminate taking into account the consolidated structure of CTTCs. Along the same line, Nakashima et al. [12] focused on the scatter of the flexural modulus of ultra-thin tapes by considering each rectangular and oriented tape as an equivalent square ply containing information about the size and orientation to obtain a laminated structure without resin-rich area. However, the interactions between chopped tapes with each other and with cavity edges have not yet been determined.

This study aims to predict the elastic modulus (in-plane stiffness) of CTTCs considering the mould cavity boundaries through a modified RSA algorithm. Next, the Set Voronoi Tessellation method is applied to generate an RVE based on local packing density for non-spherical particles. The elastic response is locally evaluated by Classical Laminate Theory (CLT) taking into account virtual equivalent layers based on locally present chopped tapes. Finally, it is investigated to which extent this approach is suitable to represent the orientation effects of chopped tapes related to cavity edges.

2. Modelling

In the literature, equivalent modelling techniques have been improved to predict the mechanical response of CTTCs due to the complexity of the structure [27,33]. The generating of a virtual specimen includes two main steps to achieve representative CTTC structures. The first step consists of creating equivalent layers which have local orientations and elastic properties according to random distribution and the tessellation algorithms are given in Section 2.1. After achieving the variable layers, virtual specimens are generated by stacking the determined amount of layers in the second step is explained in Section 2.2.

2.1. Randomisation and tessellation algorithms

An RSA algorithm was performed to generate the stochastic distribution [27]. A random seed point and a random angle in 2D are generated for the first placement of the chopped tapes. The orientation of the tapes was varied from 0° to 179° and a step size of 1° was chosen. The orientation of the next candidate chopped tape in a virtual filling process was located according to their neighbour chopped tapes whilst aiming to prevent overlapping. Chopped tapes were placed sequentially according to the packing procedure where an increasing number of attempts have to be made with an increasing packing density as free space is reduced. If the candidate chopped tape was deposited on already existing tapes, it was removed by the packing algorithm until a non-overlapped distribution was achieved. This process was continued for up to 4000 attempts for each candidate chopped tape to obtain highly jammed distributions. Because the sequential distribution reduces the placement possibility due to placed chopped tapes. An additional condition was added for the representation of chopped tape-cavity edges interactions of net-shaped specimens. The finite distribution area was defined as a boundary contour frame, being rectangular in our case. If the seed point of the candidate chopped tape was within the boundary, but the chopped tape's contours collided with the frame edge, it was eliminated and a new candidate position was generated. The number of iterations is a trade-off between desired packing density and computational cost. As illustrated in Fig. 1(a), boundary-related orientation effects start to dominate as the width of the frame becomes less than the length of chopped tapes. Thus, it is noted that the boundary of the distribution area has a prominent effect on orientations of chopped tapes. This algorithm is further referred to as *the bounded-RSA* algorithm in this study. The flow diagram of the bounded-RSA algorithm and the decision logic of the conditions are illustrated in Fig. 1(a). Before the algorithm was executed, the dimension of distribution area (specimen size) and chopped tape sizes were defined as initial parameters. The length and width of the chopped tapes for experimental and virtual specimens were 10 mm and 2.5 mm, respectively. Specimen dimensions of 150 by 60 mm were used.

The Set Voronoi tessellation was chosen due to its applicability to the rectangular shape of chopped tapes after comparing it to the conventional Voronoi Tessellation. The desired number of iterations was also defined to obtain a perfectly non-overlapped distribution for one layer. The tessellation was generated according to seed points (red and blue points in Fig. 1(b), respectively) for the conventional Voronoi whereas points of the bounding surface of tapes (blue and red points in Fig. 1(b), respectively) were employed to implement the Set Voronoi tessellation. As shown in Fig. 1(c), the area of the tape exceeds the green area that represents the cell area and some regions of other tapes are included in it. The conventional Voronoi tessellation is therefore not useful for further processing. However, the chopped tape is enclosed completely via the Set Voronoi tessellation. Based on the Set Voronoi tessellation, we define the ratio between the chopped tape area ($A_t = l_t.w_t$) and the area of its corresponding cell (A_c) [36]. This ratio is called the local packing density (ϕ) as given in Eq. (1).

$$\phi = \frac{A_t}{A_c}, \tag{1}$$

As given in Fig. 2(a), the distribution of chopped tapes is shown with a colour scale to differentiate the individual orientation angle of the chopped tapes after the filling algorithm.

These local packing density values are scalar numbers between theoretical bounds between 0 and 1, as shown in Fig. 2(b). The average local packing density for each layer of virtual DTs specimens is approximately equal to 0.44. This value is the average tape volume ratio of the non-overlapped DTs layers. The variability is the representation of the mesoscale material distortion and was obtained based on a Python Set Voronoi module [36], which was further extended to account for the boundary.

The elastic properties of AS4/PPS unidirectional (UD) prepreg chopped tapes (Table 1) are scaled by the local packing density (ϕ_i) of related cells and divided by the average local packing density (ϕ_{avg}) of the CTTC layer such that the average mechanical values of each CTTC layer are equal to the UD AS4/PPS composite to capture the morphological variabilities without weakening the CTTC layers. The local mechanical properties of the ith cell were calculated as:

$$E_{1i} = E_1 \frac{\phi_i}{\phi_{avg}}, \tag{2}$$

$$E_{2i} = E_2 \frac{\phi_i}{\phi_{avg}}, \tag{3}$$

$$G_{12i} = G_{12} \frac{\phi_i}{\phi_{avg}}, \tag{4}$$

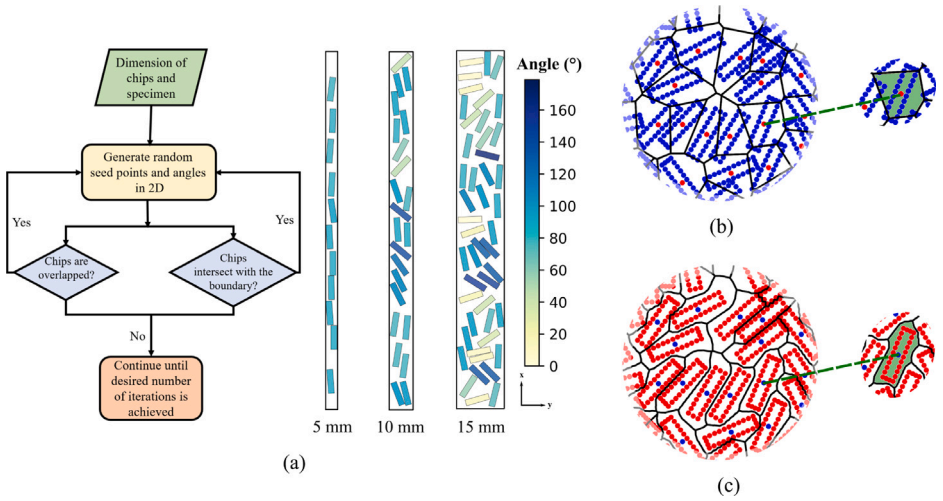

Fig. 1. (a) The bounded-RSA algorithm flowchart explains the filling sequence and shows results for specimen widths (b) The Conventional Voronoi Tessellation and resulting area in the cell, (c) The Set Voronoi Tessellation with its corresponding cell area.

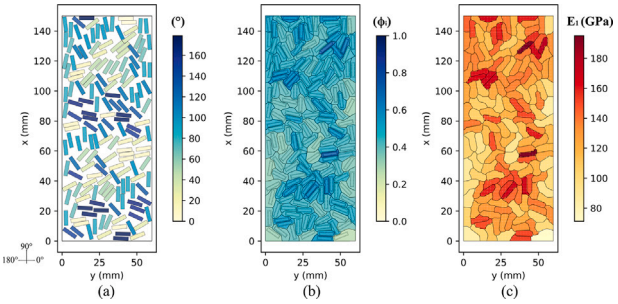

Fig. 2. A virtual DTs layer showing (a) the bounded-RSA, (b) The Set Voronoi Diagram (c) The homogenised Modulus in fibre direction E_1 within each cell.

Table 1
Elastic properties of AS4/PPS composite with a fibre volume ratio of 59% [37].

Longitudinal modulus, E_{11}	128 GPa
Transverse modulus, E_{22}	10.1 GPa
Shear modulus, G_{12}	5.7 GPa
Longitudinal Poisson's ratio, ν_{12}	0.37

$$\upsilon_{1i} = \upsilon_{12}, \upsilon_{21}\frac{\phi_i}{\phi_{avg}} \quad (\upsilon_{12i}, \upsilon_{21i} \leq 0.49), \tag{5}$$

The local elastic properties of the chopped tapes are scaled according to the equations given above. The allocation of modified Young Modulus in the fibre direction for one CTTC layer and the discretisation of the cells to the partitions are shown in Fig. 2(c). Despite that collective behaviour with nematic-like packing is observed in Fig. 2(a) and (b), the homogenised modulus does not demonstrate a readily observable collective behaviour.

2.2. Laminate analogy and orientation tensor

Due to the RSA algorithm and the Set Voronoi tessellation method, each cell demonstrates a variable orientation angle and local packing density. After specifying the local mechanical characterisations of cells to apply CLT and to calculate the elastic modulus, each cell is discretised according to the determined grid size and 0.1 mm thickness was chosen according to the processed thickness of the tapes. The CTTC layers are then combined to generate virtual CTTC specimens as seen in Fig. 3 and CLT is applied by taking into account that each partition has its own orientation and mechanical property information.

Table 2
Longitudinal and transverse modulus results according to grid sizes.

Grid size (mm)	Number of partitions	$E_{x(avg)}$	$E_{y(avg)}$
2.0	2250	48.69	44.02
1.0	9000	48.67	43.97
0.5	36 000	48.67	43.98

Each grid was assumed as an individual laminated composite to calculate the membrane term A, coupling term B and bending term D matrices from the transformed stiffness matrix (Q):

$$A_{ij} = \sum_{k=1}^{n} Q_{ij}(z_k - z_{k-1}) \quad i,j = 1,2,6 \tag{6}$$

$$B_{ij} = \frac{1}{2}\sum_{k=1}^{n} Q_{ij}(z_k^2 - z_{k-1}^2) \quad i,j = 1,2,6 \tag{7}$$

$$D_{ij} = \frac{1}{3}\sum_{k=1}^{n} Q_{ij}(z_k^3 - z_{k-1}^3) \quad i,j = 1,2,6 \tag{8}$$

The longitudinal and transverse Modulus was evaluated regarding the laminate compliance matrix (S):

$$S = \begin{bmatrix} \alpha & \beta \\ \beta & \theta \end{bmatrix} = \begin{bmatrix} A & B \\ B & D \end{bmatrix}^{-1} \tag{9}$$

$$E_x = \frac{1}{t_s \alpha_{11}}, E_y = \frac{1}{t_s \alpha_{22}} \tag{10}$$

The sensitivity of the grid subdivision for the CLT analysis of the chopped tapes laminate was performed for grid sizes of 2 mm, 1 mm and 0.5 mm (Table 2 and Fig. 4). All grid sizes show almost equal modulus values which indicate no effect of grid size within this range of subdivisions. The grid size of 1 mm was selected to balance accuracy, clarity in material distribution pattern and computational efficiency based on Table 2 and Fig. 4.

Determination of the number of CTTC layers for proper representative models was required to perform a convergence analysis. As shown in Fig. 5, the average elastic moduli E_x and E_y increase significantly until the cumulative number of CTTC layers reaches 10 and this increase continues moderately until 20 DTs layers and eventually converges. Therefore, the number of CTTC layers was taken as 20 layers to balance the computational efficiency and accuracy of the CTTC models for the rest of the study. Evaluation parameters for all virtual CTTC specimens following were taken for 20 layers and a 1 mm grid size. It is also noticed that local variabilities in layers cause a drastic decline in global Young's Modulus from the first to the second virtual layers due to the

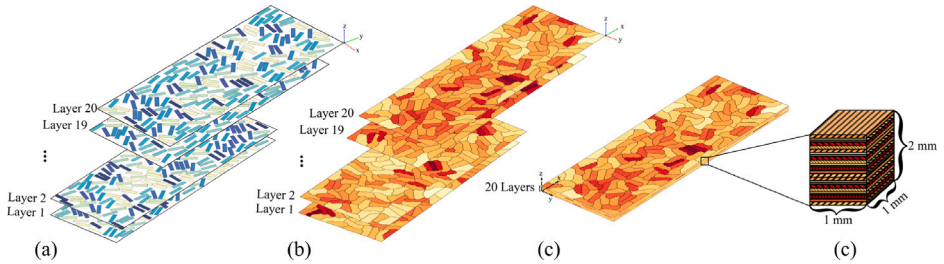

Fig. 3. Schematic representation of (a) virtual layers of non-overlapping distributions, (b) ply-wise mesoscopic variability for each virtual layer (c) assembled equivalent CTTC laminate, and (d) partition scale laminated structure.

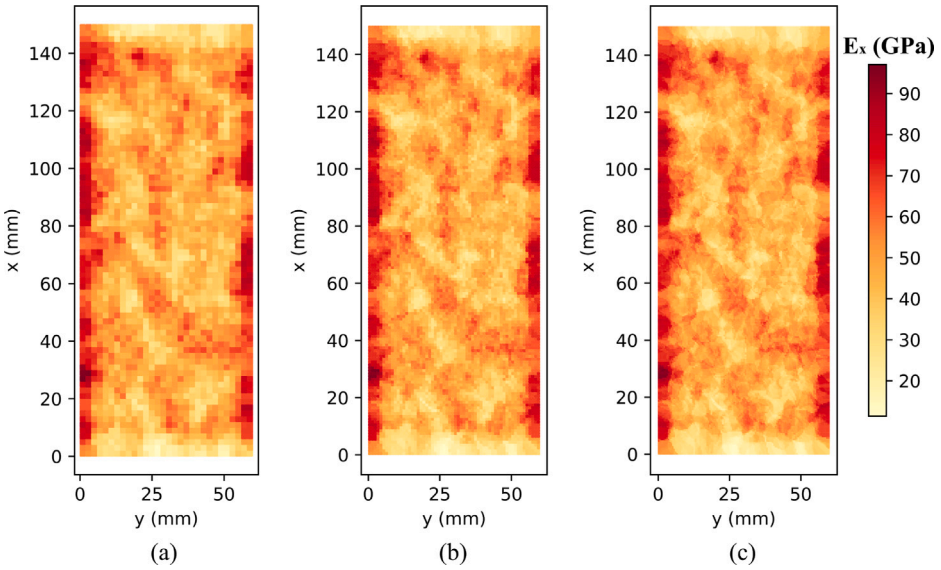

Fig. 4. Distribution of Longitudinal Modulus results according to grid sizes of (a) 2 mm (b) 1 mm (c) 0.5 mm.

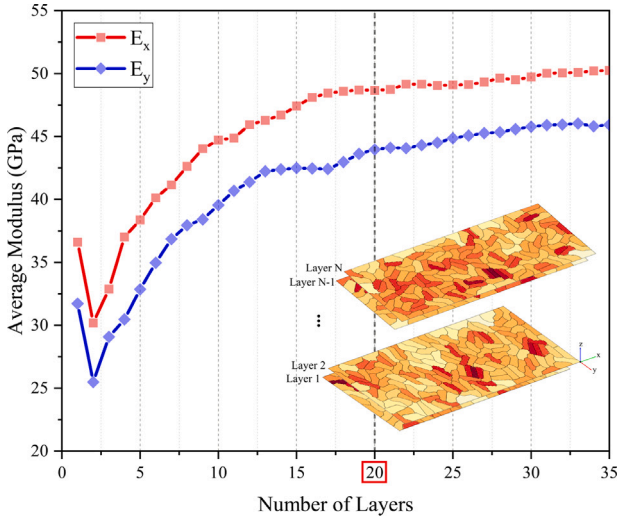

Fig. 5. Convergence analysis for the elastic moduli with respect to the number of CTTC layers.

coupling terms in the ABD matrix which is for the determination of symmetric/unsymmetric laminates through the thickness.

The second-order orientation tensor in the two-dimensional field is,

$$\alpha_{ij} = \begin{bmatrix} \alpha_{11} & \alpha_{12} \\ \alpha_{21} & \alpha_{22} \end{bmatrix} \tag{11}$$

where α_{11} and α_{22} are the orientation tensor component along the x-direction and y-direction, respectively. $\alpha_{11} = \alpha_{11} + \alpha_{22} = 1$ and $\alpha_{12} = \alpha_{21} = 0$ (α_{12} indicates the scale variation in the x and y directions.) according to the orientation state [38,39].

$$\alpha_{11} = \frac{1}{N}\sum_{g=1}^{N} \cos^2 \theta_g \tag{12}$$

where N is the number of the grid, θ_g is the angle for the gth grid in x-direction [40]. ($\alpha_{11} = 1$ means perfectly aligned, $\alpha_{11} = 0.5$ means randomly oriented distribution.)

3. Experimental details

To verify the numerical results, a compression mould with vertical shut-off for net-shaped CTTC specimens was designed as given in Fig. 6(a). The mould material was composed of Steel St60 which is durable under high pressure and high temperature. The mould consists of three main parts a frame to contour the rectangular shape and, upper and lower parts for arranging the thickness under even pressure. The cavity width, length and thickness of the mould were 60 mm, 262 mm and 2 mm, respectively. The mould was designed to manufacture CTTC specimens with thicker at the ends aiming to substitute the doublers in the clamping areas for the tensile test. This design is illustrated in Fig. 6(b), which aims to induce failure in the gauge area that measures 150 mm (highlighted in red frames) by 60 mm.

Specimens were manufactured with AS4/PPS UD prepreg chopped tapes whose dimensions in length, width and thickness were 10 mm, 2.5 mm and 0.1 mm respectively. Some specimens were tested as moulded, whereas others were tested by cutting away the part with the

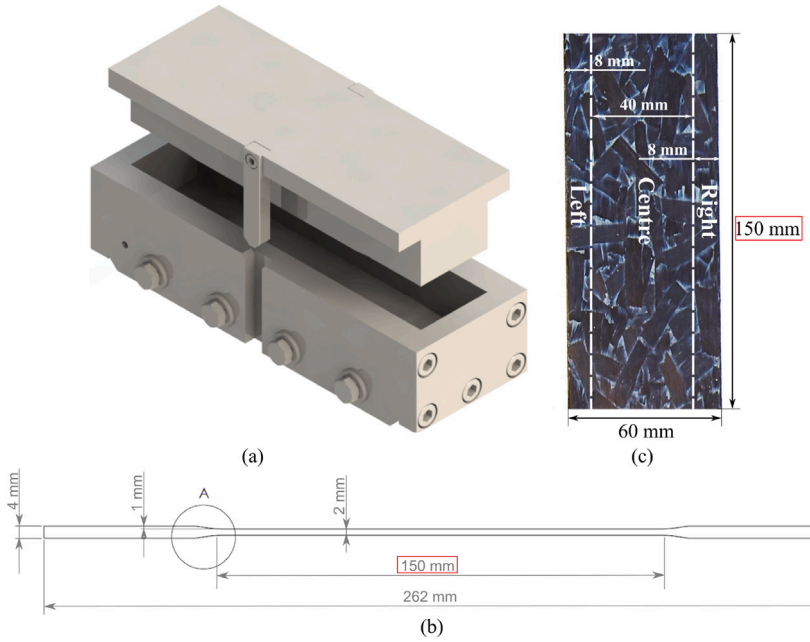

Fig. 6. (a) The net-shaped mould (b) cross-section of the mould cavity (c) representation and dimensions of gauge area in specimen.

edge-interacted mesostructures. Fig. 6(c) shows the dimensions of the edge and centre DTs specimens are 8 mm and 40 mm, respectively due to the cutting blade thickness that caused a 2 mm loss of the material while the width of the net-shaped CTTC specimens is 60 mm. For the comparison, the same dimensions are considered for the representation of the virtual CTTC specimens. A total of six experimental CTTC specimens were compared with 25 virtual CTTC specimens.

The mould was placed in the hydraulic press machine (CompoMatic A4-300) and heated to 305 °C temperature before the pressure of 25 bar was applied for 15 min. The cooling rate was 10 °C/min. A Universal Testing Machine from Walter+Bai AG with a load cell of 100 kN was used to perform the tensile loading at a rate of 2 mm/min based on ASTM D3039/D3039M-17 [41] standards for tensile properties of polymer matrix composite materials.

4. Results

Longitudinal and transverse Young modulus distributions in a CTTC specimen are depicted in Fig. 7. High scattering has been shown at the edges of the CTTC specimens in terms of Longitudinal Young modulus (Fig. 7(b)). The edge orientation is quantitatively supported by using the second-order orientation tensor in Eq. (12), shown in Fig. 8(a). Correspondingly, the edges show a highly aligned distribution whereas the rest of the CTTC specimen is placed randomly as it is seen that orientation tensors level out around 0.5, which is the same as for quasi-isotropic laminates [39]. Furthermore, the orientation tensor (green curve in Fig. 8(a)) and longitudinal Young's modulus (red curve in Fig. 8(a)) through the width of the specimen exhibit similar characteristic behaviours.

When the influence of local packing density ϕ_i on Modulus is investigated, it is noticed that a low-density fraction is observed at the edges (Fig. 8(b)). However axial Modulus is more influenced by edge-related chopped tape orientations than the drop in local packing density. As a result, the contribution of the CTTCs-cavity edges interactions to the chopped tape orientation is non-negligible to characterise the CTTCs composites.

5. Discussion

To illustrate the stochastic nature of the CTTCs, Fig. 9 shows a decrease in the coefficient of variation of the normalised Modulus and orientation tensor (α_{11}) as the number of plies in a specimen increases. When analysing Fig. 9(a), it is often important to determine at which point fluctuations stabilise and the difference between the median and mean values is minimised. In our study, we found that 16 layers was the point at which these factors converged, based on a combination of analysis techniques including the convergence of the range of fluctuations and the minimisation of the difference between the median and mean values. We also noted that the interquartile range (IQR), which represents the range between the 25th and 75th percentiles of the data, was smallest at 16 layers. A smaller IQR suggests less variation in the data within that range and implies that the data in that range is more consistent and stable, with minimal fluctuations. Furthermore, while the median and mean values do get closer after 12 layers, the difference between them is not minimised until 16 layers. Additionally, the median being slightly higher than the mean at 17 layers does not indicate a major deviation from the overall trend. If we look at the Coefficients of Variance (CoV) values based on the number of layers, we can observe a more consistent behaviour and low coefficients of variance in the distributions with a high number of layers (e.g., 16, 17, 18, 19, 20). In conclusion, based on our analysis, we determined that 16 layers were the most appropriate point to measure and analyse the data in our study. On the other hand, we can see that the median and mean values are equal at 1-layer specimens. Namely, the distribution of samples is symmetric. At the 2-layer specimens, a sudden decline appears and the range between the median and mean values increases due to the high differences between the samples in the coupling matrix B; this difference falls within variability after 16 layers. In the same manner, orientation tensors (α_{11}) based on the number of layers seem to converge after 16 layers (Fig. 9(b)). It means that a representative structure can be generated by applying the combination of a bounded RSA and the Set Voronoi Tessellation algorithms.

The most important result in Fig. 10(a) is the relation between the size of chopped tapes and the high stiffness region in the specimens. A distance of 2.5 mm from the edge of specimens, which is equal to the width of the chopped tapes, has the highest stiffness due to the high alignment. However, the alignment is still effective up to a 10 mm distance from the edges of specimens, which corresponds to the length of the chopped tapes. Furthermore, the centre region of the virtual CTTC specimens exhibited high fluctuation, while this fluctuation reduces at the edges. This relates to limited orientation

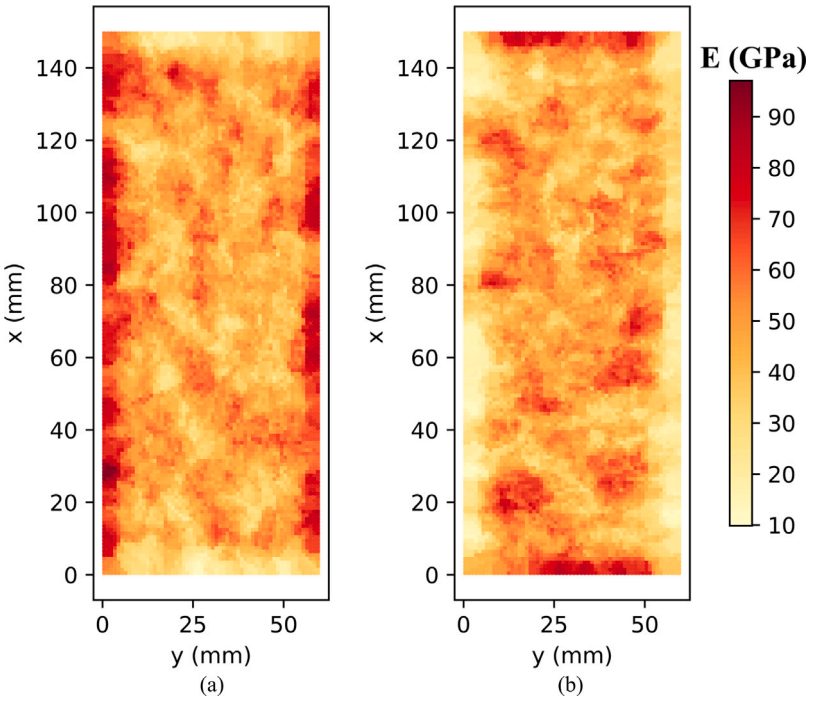

Fig. 7. Variability of (a) Longitudinal (E_x) and (b) Transverse (E_y) Young's Modulus in one virtual 20 layers CTTC specimen.

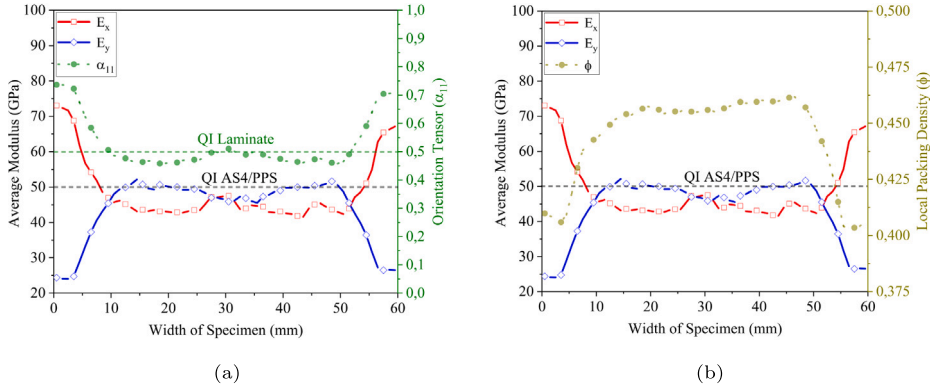

Fig. 8. (a) Orientation tensor (b) Local packing density and elasticity modulus monitored through the width of one virtual specimen (E_x, E_y, α_{11} and ϕ are the average values through the length of one virtual specimen).

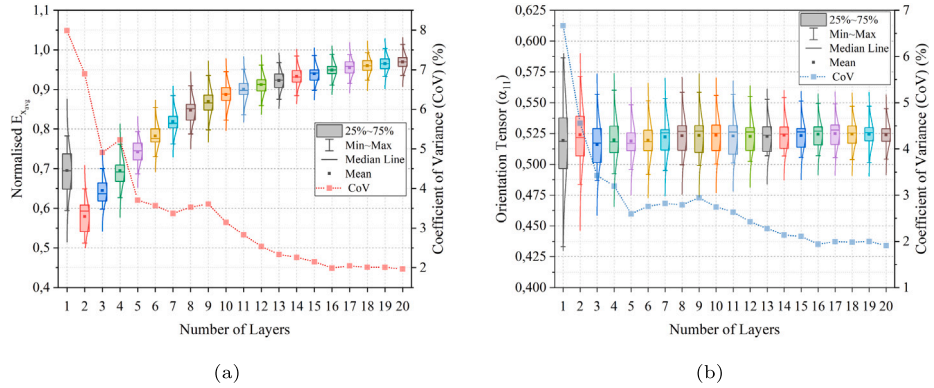

Fig. 9. Comparison of (a) normalised longitudinal Young's Modulus and (b) orientation tensor α_{11} in virtual CTTC specimens according to the cumulated number of layers.

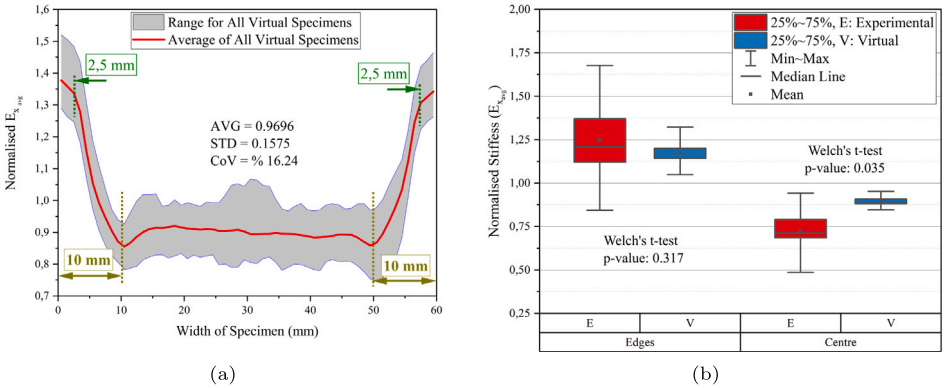

Fig. 10. (a) Deviation of normalised stiffness for all virtual CTTC specimens, also indicating the width and length of the CTTC with respect to the edge (b) Statistical comparison of experimental (E) and virtual (V) specimens measured on the sliced edges and centre regions from net-shaped CTTC specimens.

variability at the edges. Even though the standard deviation is low, the CoV is high owing to the orientation differences between the edges and the centre of the specimens, as shown in Fig. 10(a).

The apparent contribution of the edge effect to longitudinal Modulus is shown in Fig. 10(b). Numerical and experimental results have demonstrated a similar characteristic along the edges of CTTC specimens. According to Fig. 10(b), the edges in the experimental and virtual CTTC specimens present a high range between minimum and maximum values due to edge regions showing both random and highly aligned distribution, as opposed to centre regions mostly composed of a random distribution. Using Welch's t-test, which is a robust method for comparing datasets with unequal variances, the p-value obtained for the edges is 0.317. This suggests that there is statistical significance, as the p-value is higher than the commonly used threshold of 0.05 (Fig. 10(b)). While the agreement between the stiffness values at the centre of the experimental and virtual specimens may not be ideal (p-value is equal to 0.035), it is noteworthy that both types of specimens demonstrate a clear trend of decreasing stiffness from the edges towards the centre regions.

The experimental results present a higher variability than virtual specimens because of moulding and testing conditions lead to further artefacts, such as localised flow layer interruptions and the cutting process of the specimens. Nevertheless, all types of specimens have shown similar behaviour according to the regions of the specimens. Due to the transverse squeeze flow [42] and the initial placement of tapes, tapes have an increasing tendency to highly align especially at the edges [22].

Virtual specimens were generated with different lengths and a constant width (2.5 mm) of chopped tapes to understand the effect of aspect ratio (length-to-width ratio) on the Longitudinal Young Modulus. It was shown that the chopped tape-cavity edge interactions are related to the length of chopped tapes (11(a)). If the aspect ratio is equal to 1, the stiffness distribution of the CTTC specimen through its width is homogeneous. As the length of chopped tapes increases, the chopped tape-cavity edge interactions are pronounced. High aspect ratios start to enhance the stiffness of the centre of the CTTC specimens as the edge effect expands.

Specimens with a constant aspect ratio of four were generated. Chopped tape dimensions were chosen $L_t \times w_t = 10 \times 2.5, 20 \times 5, 30 \times 7.5$ (Fig. 11(b)). According to the results, we can categorise the edge effect as fully and partially dominant considering the regions of the specimens. As seen in Fig. 11(b), the range of the fully dominant chopped tape-cavity edges interactions was determined by the width of the chopped tapes, while the difference between the length and width of chopped tapes represented the range of the partially dominant chopped tape-cavity edges interactions.

The modelling technique was applied at varying mould widths from twice the width of chopped tapes (Their size is 2.5 by 10) to ten times (Fig. 12). It was shown that the narrower the mould width, the stiffer CTTC structures are obtained. Besides the dimensions of chopped tapes, the width of the mould cavity is an important parameter to tailor the mechanical performance of CTTC composites.

In Fig. 13, square net-shaped specimens of eight different sizes were generated using 2.5 mm by 10 mm chopped tapes to understand the longitudinal and transverse stiffness distributions through the x and y directions of the mould size. Characteristics of longitudinal Young Modulus through the width of the mould are similar to transverse Young Modulus through the length of the mould. The detailed figures are presented in Supplementary Material.

6. Conclusion and future work

The effects of the chopped tape-cavity edge interactions on the mechanical response and the orientation of chopped tapes have been demonstrated by a new modelling technique. The bounded-RSA algorithm was developed to prevent overlapping and consider the boundary of the distribution area and its effect on orientation followed by a Set Voronoi tessellation for generating heterogeneous layers. It is noticed that the effects of the chopped tape-cavity edge interactions on the elastic response and orientation tensor of CTTC specimens are relevant features to understanding the net-shaped CTTC specimens. The bounded RSA combined with the set Voronoi tessellation method is a suitable method to predict the mechanical properties also for complex and arbitrary boundaries. Therefore, this tessellation allows for the consideration of local variability due to the random distribution. It is demonstrated that the set Voronoi tessellation is a useful approach to implement the variability of the CTTC composites while considering the characteristic dimension of chopped tapes. While there is a quantitative discrepancy between the experimental and virtual models for the mean stiffness in the centre section, the proposed modelling approach is able to predict the increased stiffness on the edges and the spatial dependency of the stiffness based on chopped tape sizes and the dimension of the cavity. In particular, the simulations predict that the increased stiffness occurs in a region with a width similar to the length of the chopped tapes. These findings highlight the potential of this new modelling technique to further investigate and optimise chopped tape composites. Furthermore, the study suggests that specimen sizes and regions are determined according to the dimensions of the chopped tapes for the statistical reliability of the results of the experimental work. This study also demonstrates that the edge of the mould cavity has a high influence on the orientation of the chopped tapes, hence bridging the modelling gap between unidirectional and quasi-isotropic specimen configurations according to the dimensions of moulds and

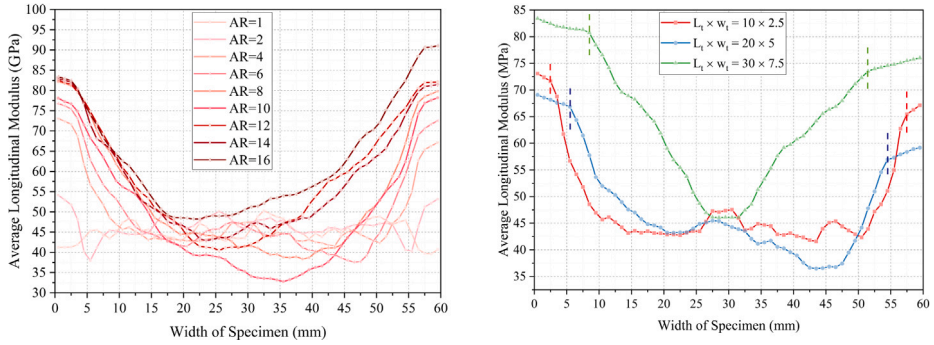

Fig. 11. (a) Longitudinal Young Modulus through the width of one CTTC virtual specimen according to different aspect ratios (b) Longitudinal Young Modulus through the width of one CTTC virtual specimen according to different chopped tape sizes with a constant aspect ratio (the dashed line indicating the specimen width).

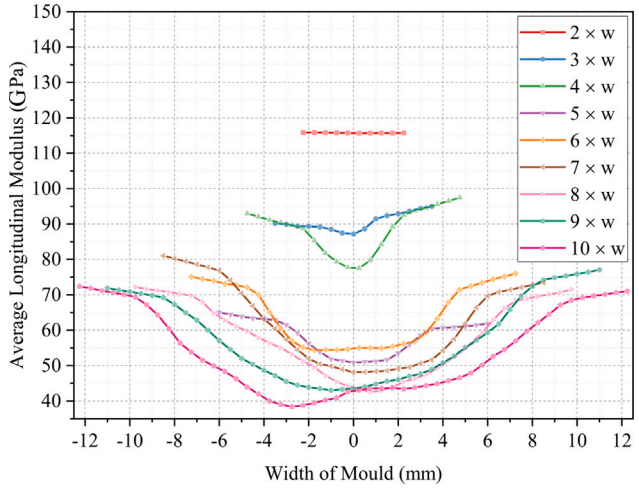

Fig. 12. Longitudinal Young's Modulus through the width of one virtual specimen according to different widths of the mould.

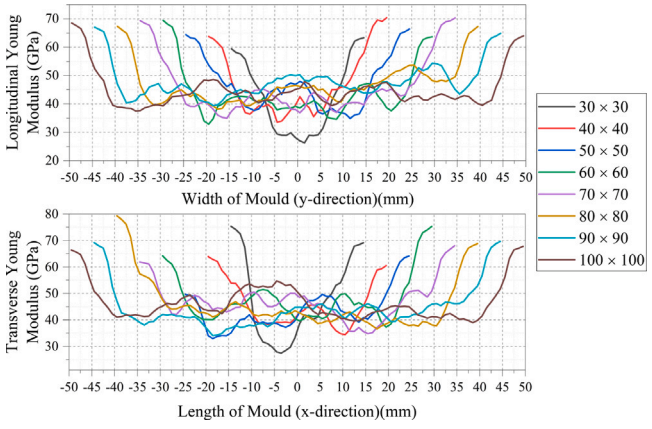

Fig. 13. Modulus distribution through the direction of the square moulds of varying sizes in mm.

chopped tapes as governing parameters. The size of the region with high stiffness is determined by the aspect ratio (length-to-width ratio) and absolute dimensions of the chopped tapes. This study contributes towards predicting the performance of complex and net-shaped CTTC components and tailoring the mechanical performance of net-shaped complex structures by mould cavity design and using chopped tapes with customised aspect ratios. Finally, this technique forms an attractive basis for Finite Element (FE) modelling to investigate the deformation and predict the failure behaviour of CTTCs.

CRediT authorship contribution statement

Deniz Ezgi Gulmez: Conceptualization, Investigation, Methodology, Software, Formal analysis, Validation, Visualisation, Writing – original draft. **Jesus Maldonado:** Investigation, Validation, Writing – review & editing. **Kunal Masania:** Conceptualization, Investigation, Validation, Writing – review & editing. **Jos Sinke:** Supervision, Writing – review & editing. **Clemens Dransfeld:** Conceptualization, Supervision, Writing – review & editing.

Declaration of competing interest

The authors declare that they have no known competing financial interests or personal relationships that could have appeared to influence the work reported in this paper.

Data availability

Data will be made available on request

Acknowledgements

We would like to thank Fraunhofer-Gesellschaft, Germany for their financial support and the Innosuisse Swiss Innovation Agency under grant number CTI 16547.1 for their financial support. We thank Christian Brauner (FHNW) for his support and Benjamin Bachman (FHNW), Nicolas Eguemann and Lian Giger (Cross Composite) for the mould design and the manufacturing of specimens and Dr. Sergio Turteltaub (TU Delft) for his valuable comments that improved the manuscript.

Appendix A. Supplementary data

Supplementary material related to this article can be found online at https://doi.org/10.1016/j.compstruct.2023.117302.

References

[1] International Council on Clean Transporation. International civil aviation organization' s CO2 standard for new aircraft. 2016, (February).

[2] The European Parliament and the Council of the European Union. Regulation (EU) 2019/631 of the European parliament and of the council of 17 april 2019 setting CO2 emission performance standards for new passenger cars and for new light commercial vehicles, and repealing regulations (EC) no 443/2009 and (EU) no 510/201. Off J Eur Union 2019;62(L111):13–53, URL http://data.europa.eu/eli/reg/2019/631/oj.

[3] Marini D, Corney JR. A methodology for near net shape process feasibility assessment. Prod Manuf Res 2017;5(1):390–409. http://dx.doi.org/10.1080/21693277.2017.1401495.

[4] Xue L, Li Y, Wang S. Direct manufacturing of net-shape functional components/test-pieces for aerospace, automotive and other applications. In: 29th international congress on applications of lasers and electro-optics, ICALEO 2010 - congress proceedings, Vol. 103. 2010, p. 479–88. http://dx.doi.org/10.2351/1.5062069, (2011).

[5] Chang IY, Pratte JF. Ldf™ thermoplastic composites technology. J Thermoplast Compos Mater 1991;4(3):227–52. http://dx.doi.org/10.1177/089270579100400302.

[6] Visweswaraiah SB, Selezneva M, Lessard L, Hubert P. Mechanical characterisation and modelling of randomly oriented strand architecture and their hybrids – A general review. J Reinf Plast Compos 2018;37(8):548–80. http://dx.doi.org/10.1177/0731684418754360.

[7] Selezneva M, Roy S, Lessard L, Yousefpour A. Analytical model for prediction of strength and fracture paths characteristic to randomly oriented strand (ROS) composites. Composites B 2016;96:103–11. http://dx.doi.org/10.1016/j.compositesb.2016.04.017.

[8] Alves M, Pimenta S. The influence of 3D microstructural features on the elastic behaviour of tow-based discontinuous composites. Compos Struct 2020;251(September 2019):112484. http://dx.doi.org/10.1016/j.compstruct.2020.112484.

[9] Sommer DE, Kravchenko SG, Denos BR, Favaloro AJ, Pipes RB. Integrative analysis for prediction of process-induced, orientation-dependent tensile properties in a stochastic prepreg platelet molded composite. Composites A 2020;130(October 2019):105759. http://dx.doi.org/10.1016/j.compositesa.2019.105759.

[10] Kravchenko SG, Sommer DE, Denos BR, Favaloro AJ, Tow CM, Avery WB, Pipes RB. Tensile properties of a stochastic prepreg platelet molded composite. Composites A 2019;124(July):105507. http://dx.doi.org/10.1016/j.compositesa.2019.105507.

[11] Yamashita S, Hashimoto K, Suganuma H, Takahashi J. Experimental characterization of the tensile failure mode of ultra-thin chopped carbon fiber tape-reinforced thermoplastics. J Reinf Plast Compos 2016;35(18):1342–52. http://dx.doi.org/10.1177/0731684416651134.

[12] Nakashima Y, Yamashita S, Zhang X, Suganuma H, Takahashi J. Analytical modelling of the behaviour and scatter of the flexural modulus of randomly oriented carbon fibre strand thermoplastic composites. Compos Struct 2017;178:217–24. http://dx.doi.org/10.1016/j.compstruct.2017.07.006.

[13] Wan Y, Takahashi J. Tensile and compressive properties of chopped carbon fiber tapes reinforced thermoplastics with different fiber lengths and molding pressures. Composites A 2016;87:271–81. http://dx.doi.org/10.1016/j.compositesa.2016.05.005.

[14] Shokrieh MM, Moshrefzadeh-Sani H. A novel laminate analogy to calculate the strength of two-dimensional randomly oriented short-fiber composites. Compos Sci Technol 2017;147:22–9. http://dx.doi.org/10.1016/j.compscitech.2017.04.034.

[15] Pimenta S, Robinson P. An analytical shear-lag model for composites with 'brick-and-mortar' architecture considering non-linear matrix response and failure. Compos Sci Technol 2014;104:111–24. http://dx.doi.org/10.1016/j.compscitech.2014.09.001.

[16] Pan Y, Iorga L, Pelegri AA. Numerical generation of a random chopped fiber composite RVE and its elastic properties. Compos Sci Technol 2008;68(13):2792–8. http://dx.doi.org/10.1016/j.compscitech.2008.06.007.

[17] Ionita A, Weitsman YJ. On the mechanical response of randomly reinforced chopped-fibers composites: Data and model. Compos Sci Technol 2006;66(14):2566–79. http://dx.doi.org/10.1016/j.compscitech.2006.01.019.

[18] Harper LT, Qian C, Turner TA, Li S, Warrior NA. Representative volume elements for discontinuous carbon fibre composites - part 2: Determining the critical size. Compos Sci Technol 2012;72(2):204–10. http://dx.doi.org/10.1016/j.compscitech.2011.11.003.

[19] Selezneva M, Roy S, Meldrum S, Lessard L, Yousefpour A. Modelling of mechanical properties of randomly oriented strand thermoplastic composites. J Compos Mater 2017;51(6):831–45. http://dx.doi.org/10.1177/0021998316654748.

[20] Harper LT, Qian C, Turner TA, Li S, Warrior NA. Representative volume elements for discontinuous carbon fibre composites - part 1: Boundary conditions. Compos Sci Technol 2012;72(2):225–34. http://dx.doi.org/10.1016/j.compscitech.2011.11.006.

[21] Shah SZ, Choudhry RS, Mahadzir S. A new approach for strength and stiffness prediction of discontinuous fibre reinforced composites (DFC). Composites B 2020;183(May 2019):107676. http://dx.doi.org/10.1016/j.compositesb.2019.107676.

[22] Tuttle M, Shifman T, Boursier B. Simplifying certification of discontinuous composite material forms for primary aircraft. In: International SAMPE symposium and exhibition (proceedings). 2010, p. 1–9.

[23] Roux M, Eguémann N, Dransfeld C, Thiébaud F, Perreux D. Thermoplastic carbon fibre-reinforced polymer recycling with electrodynamical fragmentation: From cradle to cradle. J Thermoplast Compos Mater 2017;30(3):381–403. http://dx.doi.org/10.1177/0892705715599431.

[24] Stelzer PS, Cakmak U, Eisner L, Doppelbauer LK, Kállai I, Schweizer G, Prammer HK, Major Z. Experimental feasibility and environmental impacts of compression molded discontinuous carbon fiber composites with opportunities for circular economy. Composites B 2022;234(July 2021). http://dx.doi.org/10.1016/j.compositesb.2022.109638.

[25] Hagnell MK, Åkermo M. The economic and mechanical potential of closed loop material usage and recycling of fibre-reinforced composite materials. J Clean Prod 2019;223:957–68. http://dx.doi.org/10.1016/j.jclepro.2019.03.156.

[26] Pimenta S, Pinho ST. Recycling carbon fibre reinforced polymers for structural applications: Technology review and market outlook. Waste Manage 2011;31(2):378–92. http://dx.doi.org/10.1016/j.wasman.2010.09.019.

[27] Feder J. Random sequential adsorption. J Theoret Biol 1980;87(2):237–54. http://dx.doi.org/10.1016/0022-5193(80)90358-6.

[28] Kari S, Berger H, Gabbert U. Numerical evaluation of effective material properties of randomly distributed short cylindrical fibre composites. Comput Mater Sci 2007;39(1 SPEC. ISS.):198–204. http://dx.doi.org/10.1016/j.commatsci.2006.02.024.

[29] Pan Y, Iorga L, Pelegri AA. Analysis of 3D random chopped fiber reinforced composites using FEM and random sequential adsorption. Comput Mater Sci 2008;43(3):450–61. http://dx.doi.org/10.1016/j.commatsci.2007.12.016.

[30] Duschlbauer D, Böhm HJ, Pettermann HE. Computational simulation of composites reinforced by planar random fibers: Homogenization and localization by unit cell and mean field approaches. J Compos Mater 2006;40(24):2217–34. http://dx.doi.org/10.1177/0021998306062317.

[31] Böhm HJ, Eckschlager A, Han W. Multi-inclusion unit cell models for metal matrix composites with randomly oriented discontinuous reinforcements. Comput Mater Sci 2002;25(1–2):42–53. http://dx.doi.org/10.1016/S0927-0256(02)00248-3.

[32] Chen Z, Huang T, Shao Y, Li Y, Xu H, Avery K, Zeng D, Chen W, Su X. Multiscale finite element modeling of sheet molding compound (SMC) composite structure based on stochastic mesostructure reconstruction. Compos Struct 2018;188(September 2017):25–38. http://dx.doi.org/10.1016/j.compstruct.2017.12.039.

[33] Evans KE, Ferrar MD. The packing of thick fibres. J Phys D: Appl Phys 1989;22(2):354–60. http://dx.doi.org/10.1088/0022-3727/22/2/020.

[34] Li Y, Chen Z, Su L, Chen W, Jin X, Xu H. Stochastic reconstruction and microstructure modeling of SMC chopped fi ber composites. Compos Struct 2018;200(August 2017):153–64. http://dx.doi.org/10.1016/j.compstruct.2018.05.079.

[35] Feraboli P, Cleveland T, Stickler P, Halpin J. Stochastic laminate analogy for simulating the variability in modulus of discontinuous composite materials. Composites A 2010;41(4):557–70. http://dx.doi.org/10.1016/j.compositesa.2010.01.003.

[36] Völkel S, Huang K. Set voronoi tessellation for particulate systems in two dimensions. Springer Proc Phys 2020;252(8):429–37. http://dx.doi.org/10.1007/978-3-030-55973-1{_}53.

[37] Pappas G, Canal LP, Botsis J. Characterization of intralaminar mode I fracture of AS4/PPS composite using inverse identification and micromechanics. Composites A 2016;91:117–26. http://dx.doi.org/10.1016/j.compositesa.2016.09.018.

[38] Advani SG, Tucker CL. The use of tensors to describe and predict fiber orientation in short fiber composites. J Rheol 1987;31(8):751–84. http://dx.doi.org/10.1122/1.549945.

[39] Ranganathan S, Advani SG. Characterization of orientation clustering in short-fiber composites. J Polym Sci B 1990;28(13):2651–72. http://dx.doi.org/10.1002/polb.1990.090281312.

[40] Kravchenko SG, Pipes RB. Progressive failure analysis in discontinuous composite system of prepreg platelets with stochastic meso-morphology. In: Science in the age of experience (SIMULIA User Meeting). 2018, p. 1–14, no. June.

[41] ASTM. Astm D3039/D3039M. Annual Book of ASTM Standards, 2014, p. 1–13. http://dx.doi.org/10.1520/D3039, URL http://scholar.google.com/scholar?hl=en&btnG=Search&q=intitle:Standard+Test+Method+for+Tensile+Properties+of+Polymer+Matrix+Composite+Materials#1.

[42] Advani SG, creasy TS, Shuler SF. Chapter 8 rheology of long fiber-reinforced composites in sheetforming. Compos Mater Ser 1997;11(C):323–69. http://dx.doi.org/10.1016/S0927-0108(97)80010-0.